Statistical prescission point model of fission fragment angular distributions

Bency John and S. K. Kataria
Nuclear Physics Division, Bhabha Atomic Research Centre, Mumbai-400085, India
(Received 15 October 1997)

In light of recent developments in fission studies such as slow saddle to scission motion and spin equilibration near the scission point, the theory of fission fragment angular distribution is examined and a new statistical prescission point model is developed. The conditional equilibrium of the collective angular momentum bearing modes at the prescission point, which is guided mainly by their relaxation times and population probabilities, is taken into account in the present model. The present model gives a consistent description of the fragment angular and spin distributions for a wide variety of heavy and light ion induced fission reactions. [S0556-2813(98)01203-5]

PACS number(s): 25.70.Jj, 25.70.Gh, 24.75.+i

I. INTRODUCTION

In particle induced binary fission, the physical origin of fragment angular distribution is contained in the quanta of rotational energies possessed by various rotational degrees of freedom of the fissioning nucleus at the transition state. The statistical transition state model of fragment angular distribution (TSM) based on this idea, asserts that the transition state should be the last state of thermal equilibrium for the relevant rotational degrees of freedom [1]. There has been a great deal of discussion in the literature on whether to identify this transition state with the saddle or with the scission point deformations [1–12]. In the light ion induced fission of actinide nuclei, the experimental values of angular anisotropy and their decrease with the increase in fissility of the compound nuclei, tilted the balance towards the saddle point model [12]. In the heavy ion induced fission, where high angular momentum and excitation energy states are populated, the experimental values of angular anisotropy did not allow a clear-cut conclusion regarding the question of saddle or scission point models. For these systems of high angular momentum and Z^2/A values, the saddle point model predicts small angular anisotropies since the relevant saddle point shapes are nearly spherical [13]. Statistical scission point models [4,8] in which the fate of the fission process is determined by the phase space available at the scission point, on the other hand, predict large angular anisotropies. Experimental angular anisotropy values are spread in between these predictions [9]. The high angular anisotropies observed in systems which bear characteristics of fast decay processes such as asymmetric angular distributions and incompletely relaxed mass distributions, were interpreted on the basis of quasifission (noncompound nucleus formation) [10,14]. However, there are many instances where anisotropy values are in disagreement with both saddle and scission point model predictions, even though there are no clear signatures of the fast decay processes, such as $^{28}Si+^{208}Pb$ [15], $^{16}O+^{232}Th$ [10,16], and $^{32}S+^{182}W$ [17] systems.

Another experimental approach which probes the equilibration of the fissioning nucleus is the measurement of average gamma multiplicity (M_γ) and its angular variation [18]. Since a theoretical prediction of the average total fragment spin and its possible angular dependence estimated from measured M_γ involves some of the same parameters as the fragment angular distribution, one should be able to reproduce consistently, both fragment angular anisotropy and spin, in the same model calculation. Systematic investigations in both light and heavy ion induced fissions have shown that the measured M_γ can be explained only by assuming substantial thermal excitation of the collective angular momentum bearing modes, namely, wriggling, twisting, bending, and tilting modes [19–21]. The average values of M_γ are found to be most compatible with the assumption of spin equilibrium at rather elongated configurations, comparable to those associated with the scission point [21]. Notable features of the angular variation of M_γ are that the M_γ decreases only very slowly with angle for a wide range of about $\pm 60°$ around 90°, and beyond this range, it decreases more rapidly. The overall variations does not show any systematic dependence on the fissility of the compound nuclei [21]. These features are in contrast to the predictions of the saddle point model [18].

The underlying idea of the TSM is that the complementary fragments separate along the nuclear symmetry axis and their angular distribution is given by the distribution for orientation of the symmetry axis relative to the total angular momentum vector J at the transition state [1]. The orientations of the symmetry axis depend on the values of quantum numbers J, M, and K of the available states of the transition nucleus; where M is the projection of J on a space fixed axis (taken as beam axis) and K is the projection of J on the symmetry axis. The quantum numbers J and M are conserved in the entire fission process. However, no such restriction holds for the quantum number K (the tilting spin) which in fact can be thermally excited.

According to the saddle point version of the TSM, the fissioning nucleus redistributes its energy and angular momentum in many ways during the evolution from spherical equilibrium shape to saddle point shape. This shape evolution is sufficiently slow near the saddle point such that at this point, thermal equilibrium is established for the K degree of freedom. This picture of fission process postulates that the relaxation time for the K degree of freedom is smaller than the time spent by the nucleus at the saddle point. This model further assumes that the saddle point equilibrium values of K are frozen beyond the saddle point such that these values of K can be treated as good quantum numbers for describing the fission process thereafter. This should mean either that

the duration of descent from saddle to scission has become much shorter than the time spent at the saddle point, or that the K relaxation time has increased many times for the motion beyond saddle. In either case, the saddle point model supposes a substantial change in the nature of the fission process at the saddle point. This assumption may hold good for low excitation energy fission of nuclei having moderate to large fission barriers.

For heavy ion induced fission reactions where values of spin, excitation energy, and Z^2/A are high, the fission barriers become very small. For such reactions, it is conceivable that the power of the saddle point to control the nature of the fission process is reduced considerably. Furthermore, the observation of unexpectedly large prescission neutrons in heavy ion induced fission reactions indicated that the fission is a slow process. Detailed analyses suggested that the fissioning system spends comparable times before and after the saddle point [22–26]. At the final stages of fission, if the motion in the fission direction is slow compared to the K relaxation, then one can assume K equilibration near the scission point. The present model for fragment angular distribution in fission reactions at moderate and high excitation energies, therefore, assumes near-scission-point transition states.

The concept of conditional equilibrium has several important implications for the fission studies. As already discussed, to interpret measured angular anisotropies, we need to know whether or not the reaction time was sufficiently long to allow statistical equilibration for the tilting modes. Another example is the fission probability calculation where the available phase space at the saddle point is the crucial factor. This factor is calculated under the assumption that, at the saddle point, the shape modes relax much slower than the other numerous intrinsic degrees of freedom. Prakash *et al.* [27] have extended the saddle point phase space factor calculation by assuming that the shape modes and tilting mode relax much slower than the other intrinsic degrees of freedom. In the phase space factor calculation, they have added the tilting mode energy to the potential energy of the nucleus, and at the same time, allowed thermal excitation of the tilting mode. In the present work, we adopt a similar multilayered approach for calculating the phase space factor near the scission point. Our focus will be to estimate the influences of the tilting mode on the other angular momentum bearing collective modes and account for these influences in the phase space factor calculation.

In the present work, the transition state configuration is assumed to be the prescission shape [28,29]. This configuration is just a tracing back of the scission point configuration into the internals prior to scission and contains the physics shortly before the final split. We have adopted essentials of the random neck rupture (RNR) model [28] to define the prescission shape. These shapes have turned out to be elongated, flat necked nuclei having total length to neck radius ratio of 9:1 for the compound systems studied. The rationale behind this choice is the impressive success the RNR model has achieved in describing almost all major exit channel properties of the fissioning nucleus such as mass distribution, total kinetic energy (TKE) distribution, and post neutron multiplicity distribution. In the RNR model, the exit channel properties are connected to the prescission shape via the random neck rupture hypothesis. Improvements in predicting the exit channel properties were possible since the properties of the scissioning nucleus were considered and not that of the newborn fragments. In the same spirit, to calculate fragment angular and spin distributions, the present model uses the moments of inertia and temperature parameters related only to the prescission shape. At the same time, we have not overlooked the fact that the saddle to scission region is a region of fragment formation. As stated earlier, we are considering the effects of collective rotational modes in which the forming fragments are the partners. Thus the present prescission nucleus has a dual character; it is a mono nucleus and a dinucleus at the same time. The interplay of the coherent motion of the nucleons in bulk and the internal motion of the nucleons in the nuclear field makes this possible.

Present paper is organized in the following way. In Sec. II, a description of the present model preceded by a recapitulation of the formulas used in the saddle point model and the earlier scission point models [4,8] is given. In Sec. III, experimental angular anisotropy data [10,35] are compared with the model calculations. Issues related to the fragment spins are discussed in Sec. IV. A discussion on the various facets of the present model is given in Sec. V. Finally, conclusions are presented in Sec. VI.

II. ANGULAR DISTRIBUTIONS—THEORY

In the transition state model of fission fragment angular distributions, the formula applicable for the binary fission of compound nucleus formed with angular momentum J and its projection along the beam direction $M=0$, is given by [1]

$$W(\theta)\propto\sum_{J=0}^{\infty}(2J+1)T_J\sum_{K=-J}^{J}\times\frac{(1/2)(2J+1)|D^J_{M=0,K}(\theta)|^2\rho(E^*,J,K)}{\sum_{K=-J}^{J}\rho(E^*,J,K)},\quad(1)$$

where T_J is the transmission coefficient for the partial wave J, $D^J_{M=0,K}(\theta)$ is the rotor wave function, and $\rho(E^*,J,K)$ is the level density of the transition state nucleus of excitation energy E^*, angular momentum J, and its projection on the symmetry axis K. For a deformed, axially symmetric nucleus, $\rho(E^*,J,K)$ is obtained by assuming constancy of nuclear temperature T at the transition state as

$$\rho(E^*,J,K)\propto\exp(E^*-E^{J,K}_{\rm rot})/T,\quad(2)$$

where

$$E^*=E^*_{\rm CN}-E_p-E_{\rm def},$$

E^*_{CN} is the initial excitation energy of the compound nucleus, E_p is the average excitation energy taken away by the particles emitted prior to the transition state, and $E_{\rm def}$ and $E^{J,K}_{\rm rot}$ are the deformation and rotation energies of the transition state, respectively.

In the rigid rotation limit,

$$E_{\rm rot}^{J,K}=\frac{\hbar^2 J^2}{2\mathcal{J}_\perp}+\frac{\hbar^2 K^2}{2\mathcal{J}_{\rm eff}}, \tag{3}$$

where $\mathcal{J}_{\rm eff}$ is the effective moment of inertia given by

$$\mathcal{J}_{\rm eff}=\frac{\mathcal{J}_\perp \mathcal{J}_\parallel}{\mathcal{J}_\perp-\mathcal{J}_\parallel},$$

where $\mathcal{J}_\perp$ and $\mathcal{J}_\parallel$ are the perpendicular and parallel moments of inertia, respectively, of the transition state nucleus. The first term on the right-hand side of Eq. (3) describes the lowest energy mode of rotation for a given value of J and is called yrast mode. The second term [Eq. (3)] describes the tilting mode which can be excited thermally. For convenience, we denote the first and second terms by the symbols $E_{\rm yrast}^J$ and $E_{\rm tilt}^K$, respectively.

In the case of compound nucleus reactions, J has a fixed set of values and hence Eq. (2) can be written as

$$\rho(K)\propto\exp\left(\frac{-K^2}{2K_0^2}\right), \tag{4}$$

where

$$K_0^2=\frac{T\mathcal{J}_{\rm eff}}{\hbar^2},$$

and the energies $E_{\rm CN}^*, E_p, E_{\rm def}$, and $E_{\rm yrast}^J$ assume constant values. This form of $\rho(K)$ has been used universally in the saddle point TSM where $\mathcal{J}_{\rm eff}$ and T are calculated for the saddle point configuration.

In the scission point TSM due to Rossner *et al.* [8], $\rho(K)$ is derived by assuming statistical partition of initial angular momentum J of the fissioning nucleus into orbital angular momentum l and channel spin s of the two primary fission fragments; where $l+s=J$ and K is defined as the projection of s on the symmetry axis. The channel spin s is the vector sum of spins of the two fragments, j_1 and j_2. The $\rho(K)$ in this model, is equivalent to that derived for an extended TSM model, in which the effective moment of inertia and temperature are that of a dinucleus consisting of attached spheroids joined on the long axis. For the symmetric split,

$$\rho(K)=\exp\frac{-K^2}{2S_0^2}, \tag{5}$$

where

$$S_0^2=(2I_\parallel T/\hbar^2)[(2I_\perp+\mu R_c^2)/(\mu R_c^2+2I_\perp-2I_\parallel)],$$

where $I_\parallel$ and $I_\perp$ are the moments of inertia for a single fission fragment rotating about an axis parallel and perpendicular to its symmetry axis, respectively, μ is the reduced mass of the fission channel, and R_c is the distance between the centers of the fission fragments at the scission configuration.

In the scission point TSM due to Bond [4], very similar assumptions were made regarding the channel spin s. For high J systems and for symmetric splits, he gave an expression for $\rho(K)$ as

$$\rho(K)=\exp\frac{-K^2}{2\sigma_\parallel^2}, \tag{6}$$

where

$$\sigma_\parallel^2=\frac{2\mathcal{J}_\parallel T}{\hbar^2}.$$

Here, $\mathcal{J}_\parallel$ and T are calculated for a dinucleus consisting of attached spheroids joined on the long axis.

In the above mentioned scission point transition state models, the nature of thermally excited collective rotational modes (which are responsible for the channel spin s) viz., wriggling, twisting, and bending modes, were not considered in any detail. This can be allowed only under the assumption that these modes achieve quick relaxation [30]. In these models, it has been assumed implicitly that these modes are excited irrespective of values of K.

A. Thermally excited rotational modes

It is worthwhile examining various thermally excited rotational modes that occur in a prescission nucleus and the estimates of their relaxation times. These modes are built on the yrast mode which is the minimum energy mode. The tilting mode (K) is excited by the Coriolis coupling induced by orbital rotation [30], and is manifested as an angular momentum component along the nuclear symmetry axis. The twisting, wriggling, and bending modes are excited by the fast elementary nucleon transfer process [30]. These modes [31,32], while conserving the total angular momentum, impart angular momenta to the *future* fragments. These modes are illustrated schematically in Figs. 1(a)–1(d). The thin arrows indicate the velocity fields associated with these modes. The bold arrows show the directions of the spins imparted. The doubly degenerate wriggling mode in fact paves way for the formation of the future fragments. The wriggling motion will generate equal spins in both the future fragments perpendicular to their symmetry axes. The fragment spins thus generated will be in the same direction [Fig. 1(c)]. To conserve the total angular momentum, the system as a whole rotates such that it acquires an angular momentum having magnitude equal to that of sum of future fragment spins, and direction opposite to that of future fragments. The perpendicular rotations generated in the future fragments around their center of mass will tend to break the axial symmetry but the counter rotation around the center of mass of the whole system will restore this symmetry. In the twisting mode [Fig. 1(b)], the equal spins generated in the future fragments are opposite in direction but are along the symmetry axis. The axial symmetry of the deformed nucleus is retained even after excitation of this mode. In the bending mode, the collective rotation will impart equal angular momenta in the two fragments perpendicular to their symmetry axis but in opposite directions [Fig. 1(d)]. This mode, if excited, will break the axial symmetry of the prescission nucleus because a symmetry restoring counter rotation is absent here. Large restoring force against the axial symmetry breaking is expected to suppress this mode in a strong necked nucleus. Therefore, we assume very low probability for the excitation of bending mode in the prescission nucleus.

Quantitative estimates of the relaxation times of the rotational modes discussed above are not available, nevertheless,

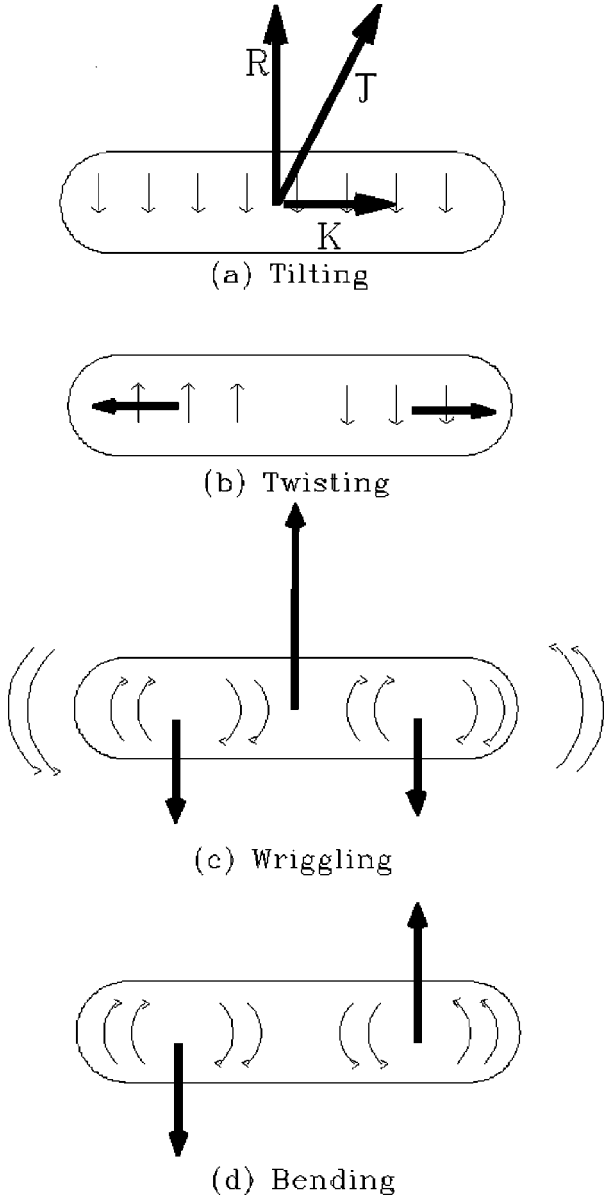

FIG. 1. (a)–(d) Schematic illustrating the collective angular momentum bearing modes for the prescission point model. The thin arrows indicate the velocity fields associated with these modes. The bold arrows show the directions of the spins imparted. In case (a), the vectors J, R, and K show the total angular momentum, orbital angular momentum, and tilting angular momentum, respectively, of the fissioning nucleus.

estimates reported for nucleus-nucleus collisions where these modes are excited, can be used as guide lines. In Ref. [30], the dynamical evolution of a dinucleus formed in a nucleus-nucleus collision is discussed in terms of the time-dependent relaxation times associated with the rotational modes. For the fission case, where scope for particle exchange between two forming fragments is large till the final split, meaningful comparisons can be made with the local relaxation times calculated for the turning point of relative motion in the nucleus-nucleus collision [30]. It has been shown in Ref. [30] that for angular momentum values typical of heavy ion induced fission reactions, the relaxation time for the tilting mode is fairly long as compared to the other nucleon transfer induced modes. Typically, the relaxation time for the tilting mode is around 2.10^{-20} sec whereas for the fast modes this time is around 3.10^{-22} sec. This may be compared with the total fission time, which is interpreted as the time needed for the considerable collective rearrangement of the system. A typical value of the total fission time estimated after considering the dynamics of the process is about 1.10^{-19} sec [24].

If the fissioning system spends about one-fifth of the total fission time near the scission point, one can assume K equilibration near the scission point. The relaxation times for the fast modes are much smaller than the K relaxation time so that the fissioning system allows equilibration of the fast modes for a given value of K. It is natural to expect that, in such conditional equilibrium, the K spin will exert influence on the excitation of the fast modes. As a result of this influence, the population of the fast modes will not be irrespective of values of K but will depend on them.

The present model takes into account this hitherto neglected dependence. This has been done by calculating $E_{\rm rot}^{J,K}$ and T in the formula for $\rho(E^*,J,K)$ [Eq. (2)], taking into account the additional energy locked in the fast modes as a function of K. Few simplifying assumptions which have been made to solve this complex problem are discussed in the following subsection.

B. Calculation of $\rho(E^*,J,K)$.

We consider only symmetric fission throughout the present calculation. The matter distribution in the two future fragments, which are equal in size, are characterized by their parallel ($\mathcal{J}_{1/2\|}$) and perpendicular ($\mathcal{J}_{1/2\perp}$) moments of inertia. In the present model, these quantities are related to the prescission shape rather than the shapes of the newborn fragments, as

$$\mathcal{J}_{1/2\|}=\frac{1}{2}\mathcal{J}_{\|},$$

and

$$\mathcal{J}_{1/2\perp}+\mathcal{J}_{1/2\perp}+\mathcal{J}_{\rm rel}=\mathcal{J}_{\perp},$$

where $\mathcal{J}_{\|}$ and $\mathcal{J}_{\perp}$ are parallel and perpendicular moments of inertia, respectively, of the prescission shape, and $\mathcal{J}_{\rm rel}$ is the relative moment of inertia of the two future fragments.

Average intrinsic spins of the future fragments K_1 and K_2 come from their share of tilting mode angular momentum K with the constraint $K=K_1+K_2$ [4,8]. For symmetric fission, $K_1=K_2=K/2$. As stated earlier, the twisting mode populates nonoscillatory intrinsic angular momentum $K_{\rm twi}$, in each of the future fragments. Sum of the rotational energies associated with the twisting mode in the two fragments is given by

$$E_{\rm twi}=\frac{K_{\rm twi}^2}{\mathcal{J}_{1/2\|}}. \tag{7}$$

The population probability for $K_{\rm twi}$, $P(K_{\rm twi})$, can be written in the form of a Boltzmann factor $\exp(-E_{\rm twi}/T)$ only if *all* modes relax quickly [30]. In this case $P(K_{\rm twi})$ will be independent of values of K. But we consider cases in which the twisting mode contributes to the intrinsic spin of the future fragments in addition to the tilting mode contribution; in other words, conditional equilibration of the twisting mode. At first let us consider the case if $K=0$; the ensuing conditional equilibration of the twisting mode will result in

equivalent velocity fields in the two future fragments. Secondly, if K is nonzero, after achieving the conditional equilibrium, the velocity field in one future fragment will be much stronger than the others. By overlapping Fig. 1(a) and Fig. 1(b) one can visualize the above two situations. Because of the velocity field mismatch, the second situation will be less probable than the first. This mismatch will be severe for larger values of K. Thus the population probability of $K_{\rm twi}$ will be reduced for larger values of K. Dependence of this reduction in probability on the value of K, temperature, and moment of inertia of the future fragments can be calculated as

$$f=\exp-\left[\frac{(K/2+K_{\rm twi})^2}{2\mathcal{J}_{1/2\|}}-\frac{(K/2-K_{\rm twi})^2}{2\mathcal{J}_{1/2\|}}\right]\Big/\,T_K. \quad (8)$$

The numerator in the exponential term [Eq. (8)] is the difference in rotational energies of the two future fragments after ''coupling'' the tilting and twisting modes. The denominator T_K is the prescission temperature corrected for the energy locked in the tilting mode K, beside other correction factors. On simplification,

$$f=\exp\frac{-KK_{\rm twi}}{\mathcal{J}_{1/2\|}T_K}. \quad (9)$$

The probability for occurrence of the prescission nucleus having a value of twisting mode angular momentum $K_{\rm twi}$, is now given by

$$P_K(K_{\rm twi})=\exp\frac{-K_{\rm twi}^2}{\mathcal{J}_{1/2\|}T_K}\exp\frac{-KK_{\rm twi}}{\mathcal{J}_{1/2\|}T_K}=\exp\frac{-K_{\rm twi}(K_{\rm twi}+K)}{\mathcal{J}_{1/2\|}T_K} \quad (10)$$

which is K dependent.

To calculate the average twisting mode energy for a given value of K, one needs to know $\langle K_{\rm twi}^2\rangle_K$ which can be obtained by taking average using Eq. (10) as a probability density function. Sum of the twisting mode energy in the two future fragments for a given value of K is given by

$$E_{\rm twi}^K=\frac{\langle K_{\rm twi}^2\rangle_K}{\mathcal{J}_{1/2\|}}. \quad (11)$$

The twisting mode introduces *fluctuations* in the values of *intrinsic spin* in the two future fragments, keeping the total intrinsic spin K of the fissioning system unchanged. Figure 2 shows the relative probability distribution function of $K_{\rm twi}$ for $K=0$, 3, and 10 $\hbar$ units for a typical value of the product $\mathcal{J}_{1/2\|}T_K\sim 50\hbar^2$. Width of the twisting mode distribution is largest for $K=0$. As K is increased, the width decreases. In the limiting cases of very large and very small twisting mode widths, the spin-dependent part of the level density of one of the future fragments can be expressed as the following equations.

The limiting case of zero width corresponds to a fixed value of K_1 or a single intrinsic spin state. In such a case [4],

$$\rho(j)\propto\exp\frac{-(j+1/2)^2}{2\sigma_\perp^2}, \quad (12)$$

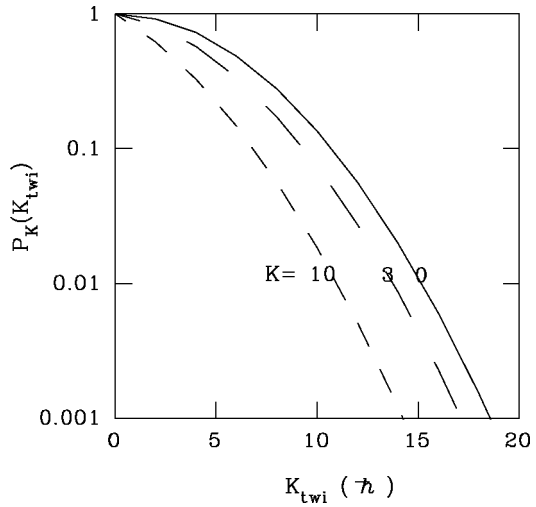

FIG. 2. Relative probability for occurrence of the prescission nucleus as a function of twisting mode angular momentum $K_{\rm twi}$. The continuous, long dashed, and dashed lines show this probability for the prescission nucleus having tilting mode spins 0, 3, and 10$\hbar$ units, respectively.

where $\sigma_\perp^2$ is the spin cutoff parameter given by $\sigma_\perp^2=\mathcal{J}_{1/2\perp}T/\hbar^2$.

For very large widths, the spin-dependent part of the level density can be obtained by summing over all allowed intrinsic spin states [33]. Then,

$$\rho(j)\propto(2j+1)\exp\frac{-(j+1/2)^2}{2\sigma_\perp^2}, \quad (13)$$

which gives a $(2j+1)$ times increase over single intrinsic-spin-state level density. This $\rho(j)$ has the same form as the spin-dependent part of the level density for a spherical nucleus. This similarity can be understood from the fact that large width of K_1 implies spherical nature. For intermediate widths, the increase will not be $(2j+1)$ times but a fraction of it, which in the present model is obtained by scaling with the width.

In addition to the twisting mode, there are wriggling modes populated in the fissioning nucleus and their conditional equilibration has to be taken into account. As stated earlier, the wriggling modes induce rotations in both the future fragments perpendicular to their axes of symmetry. The average squared magnitude of such rotations in one future fragment $\langle R_{\rm wri}^2\rangle$, can be calculated using the relation [34]

$$\langle j^2\rangle=\langle R_{\rm wri}^2\rangle+\langle K^2\rangle_{\rm th}, \quad (14)$$

where

$$\langle j^2\rangle=\frac{\Sigma j^2\rho(j)}{\Sigma\rho(j)},$$

and $\langle K^2\rangle_{\rm th}=|K/2|^2+\langle K_{\rm twi}^2\rangle$ the average squared total intrinsic spin which include the twisting mode contributions.

The sum of the average wriggling mode energies of the two fragments, for a given value of K, is given by

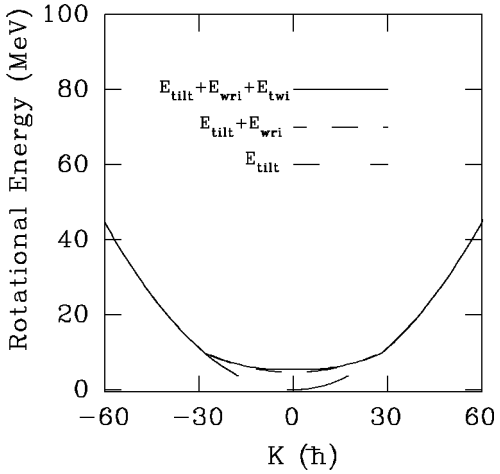

FIG. 3. Rotational energy of thermally excited collective modes for a prescission nucleus of mass $A=225$ and temperature $T=2$ MeV, as a function of tilting mode angular momentum K. Breakup of the rotational energy contributions are shown in the panel.

$$E^K_{\rm wri}=\frac{\langle R^2_{\rm wri}\rangle}{\mathcal{J}_{1/2\perp}}+\frac{2\langle R^2_{\rm wri}\rangle}{\mathcal{J}_\perp}. \tag{15}$$

Equations (11) and (15) give the average twisting mode energy and the average wriggling mode energy, respectively, for a given value of K. The total rotational energy as a function of J and K is obtained by adding these rotational energies to the yrast and tilting energies [Eq. (3)] as

$$E^{J,K}_{\rm rot}=E^J_{\rm yrast}+E^K_{\rm tilt}+E^K_{\rm twi}+E^K_{\rm wri}. \tag{16}$$

Figure 3 shows $E^K_{\rm tilt}$,$(E^K_{\rm tilt}+E^K_{\rm wri})$, and $(E^K_{\rm tilt}+E^K_{\rm wri}+E^K_{\rm twi})$ as a function of K as long dashed, dashed, and continuous lines, respectively. These quantities have been calculated for a prescission nucleus of mass $A=225$ and temperature $T=2$ MeV. It may be noted that the trough formed in the K versus $E^K_{\rm tilt}$ plot is smeared considerably by the inclusion of the fast modes, and also that the contribution to the $E^{J,K}_{\rm rot}$ from the wriggling mode is quite large compared to that from the twisting mode.

Substitution of $E^{J,K}_{\rm rot}$ [Eq. (16)] in Eq. (2) allows one to calculate $\rho(E^*,J,K)$. The resulting $\rho(E^*,J,K)$, after expansion will not have the commonly assumed Gaussian K distribution. Using $\rho(E^*,J,K)$, one can calculate the fragment angular distribution by using Eq. (1).

III. ANGULAR DISTRIBUTIONS—COMPARISON TO EXPERIMENTAL DATA

Experimental angular anisotropy data [10] for an extensive series of heavy ion reactions leading to compound nuclei in the fissility range of 0.76 to 0.88 and initial temperature range of 1 to 4 MeV have been used for comparison with present theoretical predictions. The ^{4}He+^{238}U reaction, which is one of the very few light ion systems for which anisotropy data are available over a wide range of initial temperatures [35], has also been included in the comparison.

The entrance channel spin distribution to be given as an input in Eq. (1), is contained in the spin-dependent cross section given by

$$\sigma_J=\pi\lambda\!\!\!^{-2}(2J+1)T_J, \tag{17}$$

where $\lambda\!\!\!^{-}$ is the reduced wave length and T_J is the transmission coefficient for the partial wave J. The total fusion cross section is given by the relation $\sigma_{\rm fusion}=\Sigma^\infty_{J=0}\sigma_J$. Since the present systems are highly fissile, we have used the experimental fission cross sections [10,35] as a reasonable approximation for the fusion cross sections.

The form of the transmission coefficient was taken to be

$$T_J=\left[1+\exp\frac{J-J_{\rm max}}{\Delta}\right]^{-1}, \tag{18}$$

where $J_{\rm max}$ was determined by matching the total fission cross section. The J-diffuseness parameter $\Delta(\hbar$ unit) was calculated using the approximate relation [36]

$$\Delta=\frac{k\alpha(1-E_B/2E)}{(1-E_B/E)^{1/2}}, \tag{19}$$

where α is the diffuseness of the nuclear surface, k is the wave number $(k=1/\lambda\!\!\!^{-})$,E is the incident energy, and E_B is the Coulomb barrier in the entrance channel. The value of α was taken as 0.35 fm for all the systems.

The flat necked prescission shapes of compound nuclei formed in the reactions were calculated using the dumbbell shape parameters σ_0 (elongation) and σ_2 (constriction) [37]. For each compound nucleus, the liquid drop model (LDM) potential energy surface was generated and the minimum energy trajectory or the LDM valley was computed. Among the shapes along the LDM valley, the prescission shape is defined using the relation $2l=9r$ [28], where l is the half length and r is the neck radius of the dumbbell shaped nucleus. For all compound nuclei studied in the present work, the prescission shape corresponded to $\sigma_0=2.4$ and $\sigma_2=0$. The values of $E_{\rm def}$ were calculated as the difference between potential energies of the prescission shape and of the spherical shape. The radius parameter r_0 and the surface tension coefficient γ used in all calculations were 1.16 fm [38], and $1.02\{1-1.79[(A-2Z)/A]^2\}$MeV fm^{-2}, respectively.

Consistency of the total length of the prescission shape $2l$, with the experimental mean TKE values was checked following Ref. [29]. The net energy of repulsion between the two newborn fragments, which should be approximately equal to the mean TKE, was calculated using the embedded spheroid approximation [29]. The experimental mean TKE was obtained from the Viola systematics [39]. Table I lists these two quantities for few systems. The agreement between them is reasonably good. The use of the refined parameters suggested in Ref. [28] for the prescission shape is not expected to change significantly the relevant moments of inertia and temperature parameters discussed in Sec. II B and hence was not attempted.

The energy taken away by the prescission particles E_p, was calculated by assuming only neutron emission, and using the relation [40]

TABLE I. Calculated and experimentally estimated total kinetic energy (TKE) and average total fragment spin $\langle S\rangle$ for few systems. TKE_{expt} is obtained from the Viola systematics [39]. $\langle S\rangle_{calc}$ and $\langle S\rangle^1_{expt}$ are obtained using Eqs. (22) and (21) (with parameters from [21]), respectively. $\langle S\rangle^2_{expt}=2M_\gamma$ where values of M_γ are taken from [21].

Reaction	TKE_{calc}	TKE_{expt}	$\langle S\rangle_{calc}$	$\langle S\rangle^1_{expt}$	$\langle S\rangle^2_{expt}$
120 MeV $^{16}O+^{208}Pb$	161	166±3	25.1	20.6	27
120 MeV $^{16}O+^{209}Bi$	164	170±3	25.4	21.8	28
120 MeV $^{16}O+^{232}Th$	187	190±3	30.2	27.0	30.3
120 MeV $^{16}O+^{238}U$	194	196±3	31.0	28.1	30.4
214 MeV $^{32}S+^{208}Pb$	189	192±3	29.4	30.9	36

$$E_p=M_n^{\rm pre}(7+1.5T),$$

where T is the nuclear temperature and $M_n^{\rm pre}$ is the prescission neutron multiplicity. The later was calculated using the systematics given in [40].

The temperature at the prescission point T was calculated using the relation $E^*=aT^2$, where E^* is the excitation energy available at the prescission point and a is the level density parameter. The mass number and deformation dependence of a was calculated according to [41]. The corrected temperature T_K was calculated in the same manner, but after subtracting the energy locked in the tilting mode K. The parameters S_0^2 [Eq. (5)] and $\sigma_\parallel^2$ [Eq. (6)] were calculated for the touching spheroids configuration obtained using the embedded spheroid approximation [29].

Throughout the present work no fits to the experimental data will be presented, rather the calculations based on the common procedure discussed above will be shown. The results of the calculations and the experimental data for heavy ion systems and $^4He+^{238}U$ system are presented in Figs. 4(a)–4(j) and Fig. 5, respectively. The short dashed and dashed lines are calculated using Bond's model [4] and Rossner's [8] model, respectively. The long dashed lines are calculated using Eq. (4) with $\mathcal{J}_{\rm eff}$ and T calculated for the prescission shape. The continuous lines are calculated using the present model. Experimental data are shown by solid circles [10,35] and plus signs [15,42]. There is a remarkable improvement in agreement between the experimental data and present model calculations compared to the other models [4,8,9]. As stated earlier, the other models overestimate the angular anisotropy by a huge margin. The improvement made by the inclusion of the twisting and wriggling energies in calculating the level density can be appreciated by comparing the long dashed and continuous lines.

Some discrepancies can be seen in the comparison of present model calculation and experimental data. Minor discrepancies as in the cases shown in Figs. 4(a)–4(g) and Fig. 5 may disappear by some slight changes in the pre-scission shapes and the associated parameters. Significant discrepancies exist in Figs. 4(h) and 4(i), especially for the low bombarding energies, which cannot be removed by simple adjustments of parameters. For $^{16}O+^{238}U$ system [Fig. 4(j)], it has been shown [42] that the increase observed in the values of anisotropy for bombarding energies below 90 MeV is due to the presence of quasifission events. Such a possibility exists for $^{32}S+^{208}Pb$, and $^{32}S+^{197}Au$ systems also, since the projectile in these cases is massive. Thus, the presence of quasifission events could be the reason for the observed discrepancies in Fig. 4(h)–4(j) at low bombarding energies.

IV. GAMMA MULTIPLICITY

Measurements of the average gamma multiplicity (M_γ) in fission reactions provide estimates of the average total fragment spin $\langle S\rangle$. The latter quantity is defined as the sum of average individual fragment spins

$$\langle S\rangle=\langle|j_1|\rangle+\langle|j_2|\rangle. \tag{20}$$

The M_γ is related to the average total fragment spin via the relation

$$\langle S\rangle=2(M_\gamma-\alpha)+\beta M_n, \tag{21}$$

where α,β, and M_n are the number of statistical gamma rays per fragment, average spin removed by one emitted neutron, and total neutron multiplicity, respectively.

According to the Bond [4] and Rossner [8] scission point models, the average total fragment spin $\langle S\rangle$ depends only on the spin cutoff parameters of the newborn fragments. In the present model, $\langle S\rangle$ depends only on the spin cutoff parameters of the future fragments through the following relation. For symmetric fission,

$$\langle S\rangle=2\langle|j|\rangle, \tag{22}$$

where

$$\langle|j|\rangle=\frac{\Sigma|j|\rho(j)}{\Sigma\rho(j)}$$

where $\rho(j)$ is calculated according to Eq. (13). In Table I, the values of average total fragment spin calculated using Eq. (22) ($\langle S\rangle_{calc}$) and the values experimentally determined [21] ($\langle S\rangle^1_{expt}$) for five heavy ion systems are given. Within about $3\hbar$ units, the theoretical and experimental values are in agreement. This is somewhat a good agreement considering the uncertainties in the parameters α, β, and M_n. To illustrate the dependence of experimentally determined $\langle S\rangle$ on these parameters, $\langle S\rangle^2_{calc}=2M_\gamma$ values are also listed in Table I.

The angular variation of M_γ is another experimental observation which theoretical models must address. Conspicuous features of the observed angular variation are that the change in M_γ as a function of the angle is small and essentially identical, for most of the systems. In the remaining part of this section, we discuss some clues on this observation, developed in the premises of the present model.

In Sec. II B, it has been shown that for smaller values of K, the twisting and wriggling modes are excited with larger probability. Among the two modes, the wriggling mode has a dominant role and is the sole provider of perpendicular spin ($R_{\rm wri}$) to the fragments. The final fragment spins originate from the coupling of these modes and the tilting mode (K). By following the method given in [18], one can disentangle the angular variation of $\langle K^2\rangle$. Reference [18] predicts that for a typical value of K_0^2 [Eq. (4)] for the present systems,

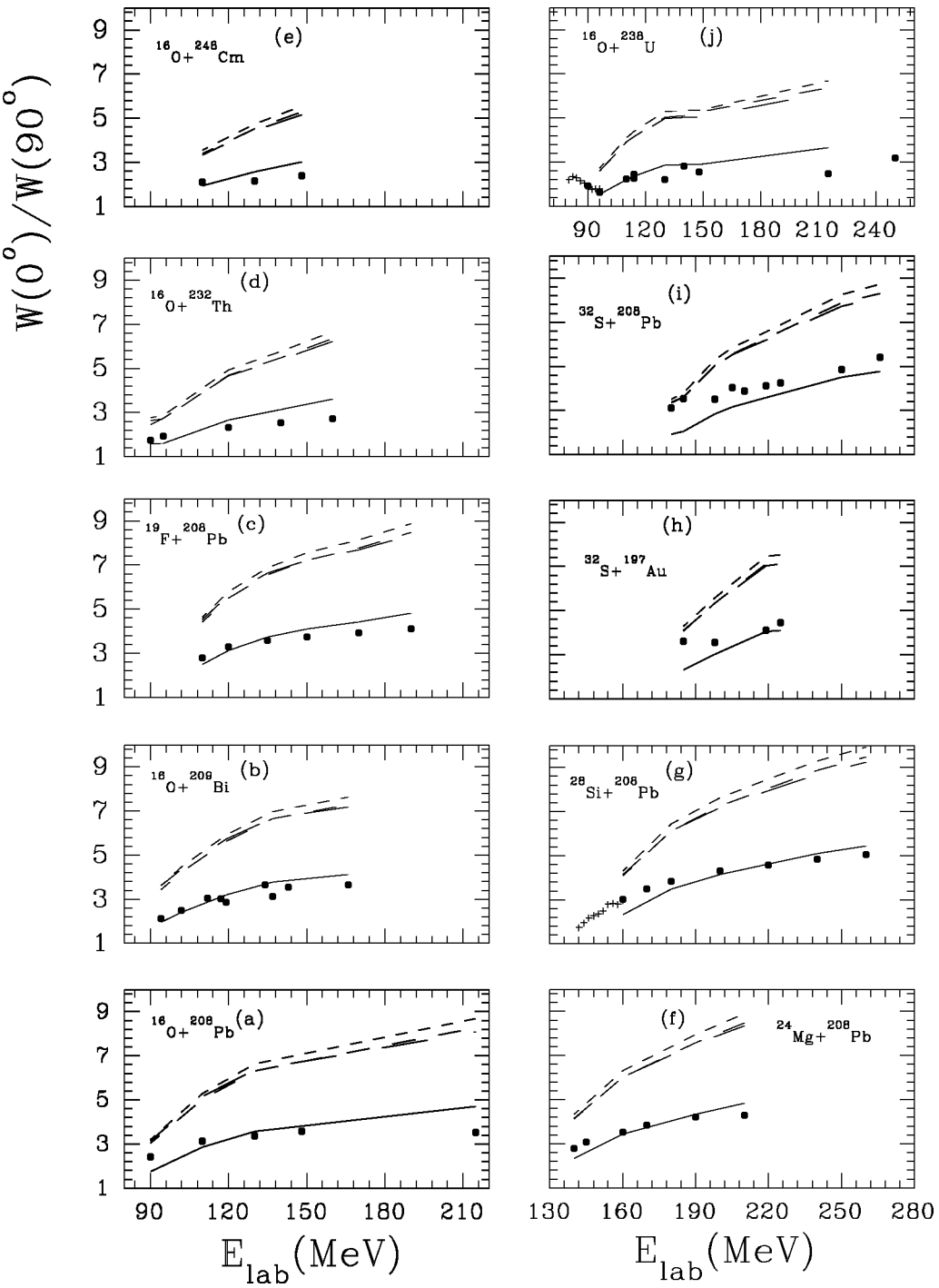

FIG. 4. (a)–(j) Angular anisotropy versus bombarding energy for heavy ion induced fission reactions. The closed circles indicate the experimental data from [10] and the plus signs indicate data from [15,42]. The lines show the result of various model calculations. The continuous lines are calculated using the present model. The short dashed, dashed, and long dashed lines are calculated after substituting Eq. (6) (Bond model), Eq. (5) (Rossner model), and Eq. (4) (Freifelder model), respectively, in Eq. (1).

$\langle K^2 \rangle$ will remain nearly a constant for a wide range of angles around 90° and then will fall off rapidly near 0° and 180°. The complementary variation of $\langle R^2_{\rm wri} \rangle$ can be obtained by using the approximate relation $\langle j^2 \rangle = \langle R^2_{\rm wri} \rangle + \langle K^2 \rangle$. This relation implies that $\langle R^2_{\rm wri} \rangle$ will be nearly a constant for the same angular range around 90°, and will increase near 0° and 180°. Thus, the present model predicts definable angular variation for the quanta of perpendicular and parallel rotations. The ratio $\langle R^2_{\rm wri} \rangle / \langle K^2 \rangle$ will not vary for a wide range of angles around 90° but will increase as 0° or 180° is approached. A point to be noted here is that the increase of the above ratio near 0° and 180° will be much larger than the case if $\langle R^2_{\rm wri} \rangle$ is angle independent [21]. One can expect that this relative variation in spin components will be retained by the newborn fragments, and the neutron emission from the fragments will carry its signatures.

It is known that the neutrons emitted from the fragments carry orbital angular momenta and impart equal and opposite

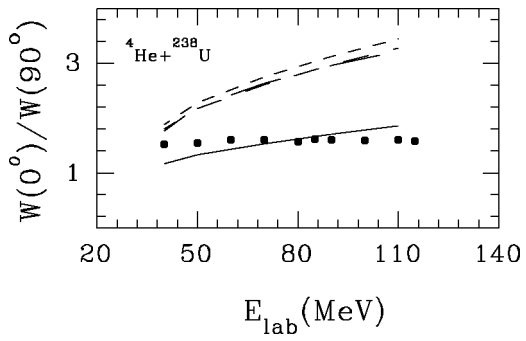

FIG. 5. Fragment angular anisotropy versus bombarding energy for the ^{4}He+^{238}U system. The symbolism and descriptions are the same as in Fig. 4. The experimental data are from [35].

angular momenta (recoil angular momenta l) to the residual fragments. If the component of l along an axis perpendicular to the symmetry axis (which passes through the center of mass of the fragment; one axis) l_1 is negative, then a part of angular momentum arising from rotations perpendicular to the symmetry axis is removed from the fragment. Similarly if the component along the symmetry axis (three axis) l_3 is negative, then a part of angular momentum arising from the intrinsic spin is removed from the fragment. For spheroidal fragments $|l_1|$ can take larger values compared to $|l_3|$, since for a given linear momentum distribution of the emitted neutrons, the average length of the radius vector is larger when measured relative to the one axis rather than the three axis.

Dietrich *et al.* [43] have worked out a simple semiclassical method to calculate the l_1 or l_3 distributions for any arbitrary deformation. The basic principle of the method is the following. The probability for emission of a neutron carrying an orbital angular momentum l and its projection on the rotation axis l_i, is controlled by the transmission coefficient $w(\epsilon,l,l_i,\chi)$ and the phase space factors. In the argument list of the transmission coefficient, ϵ, l, and l_i represent the energy, orbital angular momentum, and its projection along the rotation axis i of the emitted neutrons, respectively, and χ stands for all quantities not explicitly mentioned such as mass, nuclear deformation, and direction in space in which the particles are emitted. We have calculated l_1 and l_3 distribution using this prescription, for a typical spheroidally deformed fragment of mass number 115 and axis ratio 1:1.9.

Figure 6(a) shows the calculated transmission coefficients as a function of l_1 and l_3, for fixed values neutron energy ($\epsilon=5$ MeV) and recoil angular momentum ($l=2\hbar$). The presented values are normalized for the purpose of comparison. Figure 6(b) shows the calculated transmission coefficients, normalized after averaging over all possible l values with average transmission coefficients w_l as weights, and over all possible values of ϵ with neutron energy spectra $N(\epsilon)$ as weights. As expected, the l_3 distribution is considerably narrower than the l_1 distribution. [In the above calculations, $N(\epsilon)$ was obtained by assuming excitation energy of the fragment as 30 MeV. The average value of the transmission coefficient w_l was calculated by averaging $w(\epsilon,l,l_1,\chi)$, over allowed l_1 values. Figure 6(c) shows w_l as a function of l for $\epsilon=5$ MeV for the spheroidal and spherical shapes.]

From the above study on transmission coefficients of spheroidally deformed fragments, it may be noted that the neutrons can remove angular momentum more efficiently

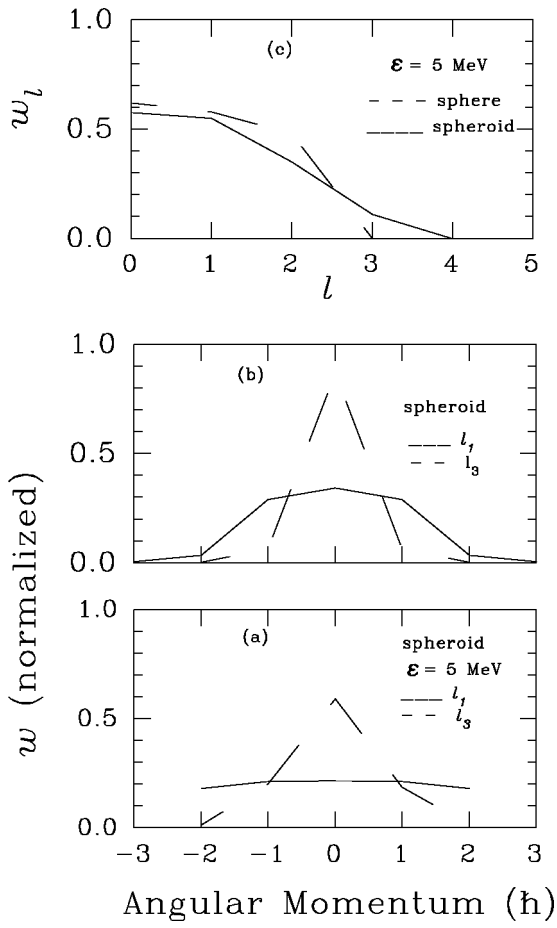

FIG. 6. Transmission coefficients for neutrons emitted from a spherical and a spheroidal (axis ratio 1:1.9) nucleus of $A=115$. Case (a) corresponds to fixed value of neutron energy $\epsilon=5$ MeV and recoil angular momentum $l=2\hbar$. Case (b) is obtained after averaging transmission coefficients over all possible values of ϵ and l. Case (c) shows transmission coefficients w_l as a function of recoil angular momentum l, for $\epsilon=5$ MeV.

from the perpendicular rotations. For a quantitative estimate of angular momentum removal, one has to consider the role of phase space which usually favor removal of angular momentum from large rotations. The present model predicts relatively large quanta of perpendicular rotations near 0° and 180° for the spheroidal fragments.

The dynamics of the shape evolution of the newborn fragments from spheroidal to spherical shape also has to be taken into account in such calculations. It may be noted that the rotational energy associated with the perpendicular rotations increases whereas the rotational energy associated with the intrinsic rotations decreases, as the fragment evolves from initial spheroidal shape to spherical equilibrium shape. Therefore, the fragments may retain intrinsic angular momentum and give away perpendicular angular momentum in neutron emissions during the evolution. We intent to perform realistic calculations to quantitatively predict M_γ as a function of angle, by including the above mentioned effects on the angular momentum removal, in a future work. The present study suggests that the angular dependence of M_γ arises mainly from post scission particle emission characteristics. If this is true, then the angular dependence of M_γ will be almost independent of the fissility of the system. The experimental data [19–21] in fact show such a trend.

V. DISCUSSIONS

Models of statistical equilibrium at the scission point have been used for many aspects of particle induced fission such as mass distribution, TKE distribution, fragment spin, excitation energy distributions, etc. However, for the fragment angular distribution there have been some reservations in using the scission point model. One of the reasons could be that the formulas derived under certain reasonable assumptions [4,8] yielded substantially higher values of anisotropy compared to the experimental data (see Fig. 4). In Refs. [4,8], an expression for calculating the anisotropy is given, for the case where the transition state configuration is assumed to be touching spheroids which are not aligned. This expression yielded anisotropy values somewhat in agreement with the experimental data [8]. However, this expression was not favored since the physical nature of the transition state configuration assumed is not realistic; one has to assume nonaxial separation of the fragments such as in the case of particle evaporation.

The *fluctuations* in the values of *intrinsic spin* of future fragments at the prescission point (Sec. II B) deserves special attention in the context of the assumption made in [4,8] on nonaxial separation of the fragments. What motivated such an assumption is the requirement of relaxation of the condition on having fixed values of intrinsic spins of the fragments. In the present model, the fluctuations introduced by the twisting mode provide variation in K states automatically. At the same time, there is no need for assuming nonaxial nature for the prescission shape. This observation apparently broadens the definition of the term transition state from that characterizes a one-dimensional process [1]. For a related discussion see [44].

The present model has the ability to treat the prescission shape as a whole, and the density of levels at the prescission point $\rho(E^*,J,K)$ takes into account the orientation of the deformed shape relative to the angular momentum vector [7]. Unlike the previous models [4,8], which assume that the statistical equilibrium of the fission axis is decided by the properties of fragments after the scission, the present model makes a more reasonable assumption [7,9] that this equilibrium is achieved at a stage prior to the final split. Although ordinary LDM predicts a steep saddle-to-scission landscape, there are many experimental results which suggest that this landscape is rather flat [45], and in that sense, the present assumption of a quasiequilibrium point near scission may be justified.

Models of statistical equilibrium at the scission point can be broadly classified according to the level of mixing of collective and single particle degrees of freedom. The one postulated by Fong [46] advocates strong mixing of *all* degrees of freedom. The Ericson model for particle evaporation from a compound nucleus [47], which is the basis of the models presented in Refs. [4] and [8], has an approach similar to Fong's model. Nörenberg's model [48] has a different approach, as it assumes a condition of intermediate mixing between the collective and single particle degrees of freedom as the system moves along the fission degree of freedom. According to Nörenberg, the mixing among collective degrees of freedom is expected to be stronger compared with that between collective and single particle degrees of freedom. The scission point model of Wilkins *et al.* [49], which is based on the assumption of statistical equilibrium among collective degrees of freedom at the scission point, is similar in many aspects to Nörenberg's model. The present model also assumes a condition of intermediate mixing between the collective and single particle degrees of freedom, however, at the prescission point.

The inclusion of the effects arising from the excitation of wriggling and twisting modes is the main factor responsible for the improved angular distribution prediction by the present model. The final fragment spins originate from the coupling of these modes and the tilting mode; therefore, a high degree of correlation between the angular distribution and final fragment spin distribution is expected. The good agreement observed between the present model calculation and the experimentally estimated average total fragment spin (Table I) points towards this correlation. The finding of Ogihara *et al.* [50] that the angular momentum coupling between the entrance and exit channels plays a decisive role on the angular distribution of the fragments is also in conformity with this expectation.

The present model can be extended for obtaining correlations between the angular anisotropy and specific exit channel properties, by the combined use of the present prescription for angular distribution and the random neck rupture (RNR) model for the exit channel. Algorithms for the usage of the RNR model are given in Ref. [29]. Let us consider the mass-asymmetry angular-anisotropy correlation at first. If the fission channel calculation of the RNR model predicts only one prescission shape for a fissioning system, then the application of the present model without any further modifications will yield the same angular anisotropy for all mass splits. However, for some systems, if several prescission shapes are predicted, then angular anisotropy should be calculated by properly weighting each prescission shape by the predicted branching ratios [29]. In such a case, a definite correlation between mass and anisotropy may emerge as a consequence of different weights for the various prescission shapes which produce mass dispersion and the associated anisotropies. Similarly, the correlation between fragment shell effects and angular anisotropy can be studied, since one can associate some magic numbers of the prescission nucleus in terms of prescission shapes with the magic numbers of the fragments [29]. Experimental studies have reported such correlations; for examples, see Ref. [16] and Refs. [3–12] cited therein.

VI. CONCLUSIONS

We have developed a model for fission fragment angular distributions, which assumes statistical equilibrium for the tilting mode at the prescission point. The conditional equilibrium of the collective angular bearing modes at the prescission point, which is guided mainly by their relaxation times and population probabilities, has been taken into account in the present model. This has brought in a hitherto neglected dependence of the population probability for the wriggling and twisting modes, on the tilting mode angular momenta. It has been found that for the tilting angular momentum (K) values near zero, the wriggling and twisting

mode contributions are maximum and as $|K|$ is increased, this contribution decreases. It has been suggested that, for calculating the fragment angular distribution using the transition state model, the phase space factor at the prescission point (transition state) should be calculated after subtracting the rotational energy locked in these modes.

Present model calculations are in reasonable agreement with the experimental angular anisotropy data for a wide variety of heavy and light ion induced fission reactions. It has been shown that the present model provides substantially improved predictions compared to the earlier scission point models. Some discrepancies observed for few systems at low bombarding energies have been attributed to the presence of quasifission reactions. The present model also provides a consistent description of the average total fragment spins estimated from the experimental M_γ data.

ACKNOWLEDGMENTS

We are grateful to Dr. S. S. Kapoor for his encouragement and fruitful discussions. We would like to acknowledge helpful discussions with Dr. D. M. Nadkarni, Dr. R. K. Choudhury, and Dr. A. K. Mohanty. We wish to express our appreciation to Dr. B. K. Jain, Dr. S. B. Manohar, and Dr. S. Kailas for their keen interest in this work.

[1] R. Vandenbosch and J. R. Huizenga, *Nuclear Fission* (Academic, New York, 1973).
[2] P. D. Bond, Phys. Rev. Lett. **52**, 414 (1984).
[3] R. Vandenbosch, Phys. Rev. Lett. **53**, 1504 (1984); P. D. Bond, *ibid.* **53**, 1505 (1984).
[4] P. D. Bond, Phys. Rev. C **32**, 471 (1985); **32**, 483 (1985).
[5] H. H. Rossner, J. R. Huizenga, and W. U. Schröder, Phys. Rev. Lett. **53**, 38 (1984).
[6] H. Fuchs, Phys. Rev. Lett. **54**, 1459 (1985); H. H. Rossner, J. R. Huizenga, and W. U. Schröder, *ibid.* **54**, 1460 (1985).
[7] T. Dø̈ssing, Phys. Rev. Lett. **54**, 1596 (1985); H. H. Rossner, J. R. Huizenga, and W. U. Schröder, *ibid.* **54**, 1597 (1985).
[8] H. Rossner, J. R. Huizenga, and W. U. Schröder, Phys. Rev. C **33**, 560 (1986).
[9] R. Freifelder, M. Prakash, and J. M. Alexander, Phys. Rep. **133**, 315 (1986).
[10] B. B. Back, R. R. Betts, J. E. Gindler, B. D. Wilkins, S. Saini, M. B. Tsang, C. K. Gelbke, W. G. Lynch, M. A. McMahan, and P. A. Baisden, Phys. Rev. C **32**, 195 (1985), and references therein.
[11] A. Gavron, P. Eskola, A. J. Sierk, J. Boissevain, H. C. Britt, K. Eskola, M. M. Fowler, H. Ohm, J. B. Wilhelmy, S. Wald, and R. L. Ferguson, Phys. Rev. Lett. **52**, 589 (1984).
[12] R. F. Reising, G. L. Bate, and J. R. Huizenga, Phys. Rev. **141**, 1161 (1966).
[13] S. Cohen, F. Plasil, and W. J. Swiatecki, Ann. Phys. (N.Y.) **82**, 557 (1974).
[14] W. Q. Shen, J. Albinski, A. Gobbi, S. Gralla, K. D. Hildenbrand, N. Herrmann, J. Kuzminski, W. F. J. Müller, H. Stelzer, J. Tōke, B. B. Back, S. Bjørnholm, and S. P. Sørensen, Phys. Rev. C **36**, 115 (1987).
[15] D. J. Hinde, C. R. Morton, M. Dasgupta, J. R. Leigh, J. C. Mein, and H. Timmers, Nucl. Phys. **A592**, 271 (1995).
[16] Bency John, Aruna Nijasure, S. K. Kataria, A. Goswami, B. S. Tomar, A. V. R. Reddy, and S. B. Manohar, Phys. Rev. C **51**, 165 (1995).
[17] B. B. Back, P. B. Fernandez, B. G. Glagola, D. Henderson, S. Kaufman, J. G. Keller, S. J. Sanders, F. Videbaek, T. F. Wang, and B. D. Wilkins, Phys. Rev. C **53**, 1734 (1996).
[18] R. P. Schmitt and M. Tirion, Phys. Rev. C **31**, 701 (1985).
[19] R. P. Schmitt, H. Dejbakhsh, D. R. Haenni, G. Mouchaty, T. Shutt, and M. Tirion, Phys. Lett. B **192**, 44 (1987).
[20] R. P. Schmitt, D. R. Haenni, L. Cooke, H. Dejbakhsh, G. Mouchaty, T. Shutt, and H. Utsunomiya, Nucl. Phys. **A487**, 370 (1988).
[21] R. P. Schmitt, L. Cooke, H. Dejbakhsh, D. R. Haenni, T. Shutt, B. K. Srivastava, and H. Utsunomiya, Nucl. Phys. **A592**, 130 (1995).
[22] G. R. Tillack, Phys. Lett. B **278**, 403 (1992).
[23] T. Wada, Y. Abe, and N. Carjan, Phys. Rev. Lett. **70**, 3538 (1993).
[24] K. Siwek-Wilczyńska, J. Wilczyński, R. H. Siemssen, and H. W. Wilschut, Phys. Rev. C **51**, 2054 (1995).
[25] J. P. Lestone, J. R. Leigh, J. O. Newton, D. J. Hinde, J. X. Wei, J. X. Chen, S. Elfstrom, and D. G. Popescu, Phys. Rev. Lett. **67**, 1078 (1991).
[26] H. Ikezoe, N. Shikazono, Y. Nagame, Y. Sugiyama, Y. Tomita, K. Ideno, A. Iwamoto, and T. Ohtsuki, Phys. Rev. C **42**, 342 (1990).
[27] M. Prakash, V. S. Ramamurthy, S. S. Kapoor, and J. M. Alexander, Phys. Rev. Lett. **52**, 990 (1984).
[28] U. Brosa and S. Grossmann, Z. Phys. A **310**, 177 (1983).
[29] U. Brosa, S. Grossmann, and A. Müller, Phys. Rep. **197**, 167 (1990).
[30] T. Dø̈ssing and J. Randrup, Nucl. Phys. **A433**, 215 (1985).
[31] J. R. Nix and W. J. Swiatecki, Nucl. Phys. **71**, 1 (1965).
[32] L. G. Moretto and R. P. Schmitt, Phys. Rev. C **21**, 204 (1980).
[33] S. Bjørnholm, A. Bohr, and B. R. Mottelson, *Proceedings of the Third International Symposium on the Physics and Chemistry of Fission*, Rochester, 1973 (International Atomic Energy Agency, Vienna, 1974), Vol. I, p. 367.
[34] R. Bock, Y. T. Chu, M. Dakowski, A. Gobbi, E. Grosse, A. Olmi, H. Sann, D. Schwalm, U. Lynen, W. Müller, S. Bjørnholm, H. Esbensen, W. Wölfli, and E. Morenzoni, Nucl. Phys. **A388**, 334 (1982).
[35] S. S. Kapoor, H. Baba, and S. G. Thompson, Phys. Rev. **149**, 965 (1966).
[36] P. E. Hodgson, *Nuclear Heavy Ion Reactions* (Oxford University Press, Oxford, 1978).
[37] R. W. Hasse and W. D. Myers, *Geometrical Relationships of Macroscopic Nuclear Physics* (Springer, Berlin, 1988).
[38] P. Möller, J. R. Nix, W. D. Myers, and W. J. Swiatecki, At. Data Nucl. Data Tables **59**, 185 (1995).
[39] V. E. Viola, K. Kwiatkowski, and M. Walker, Phys. Rev. C **31**, 1550 (1985).
[40] D. Hilscher and H. Rossner, Ann. Phys. (Paris) **17**, 471 (1992).

[41] J. Bartel, K. Mahboub, J. Richert, and K. Pomorski, Z. Phys. A **354**, 59 (1996).
[42] D. J. Hinde, M. Dasgupta, J. R. Leigh, J. P. Lestone, J. C. Mein, C. R. Morton, J. O. Newton, and H. Timmers, Phys. Rev. Lett. **74**, 1295 (1995).
[43] K. Dietrich, K. Pomorski, and J. Richert, Z. Phys. A **351**, 397 (1995).
[44] Bency John, S. K. Kataria, B. S. Tomar, A. Goswami, G. K. Gubbi, and S. B. Manohar, Phys. Rev. C **56**, 2582 (1997).
[45] M. Asghar and R. W. Hasse, J. Phys. C **6**, 455 (1984).
[46] P. Fong, Phys. Rev. **102**, 434 (1956).
[47] T. Ericson, Adv. Phys. **9**, 425 (1960).
[48] W. Nörenberg, *Proceedings of the Second International Atomic Energy Symposium on the Physics and Chemistry of Fission* (International Atomic Energy Agency, Vienna, 1969), p. 51.
[49] B. D. Wilkins, E. P. Steinberg, and R. R. Chasman, Phys. Rev. C **14**, 1832 (1976).
[50] M. Ogihara, H. Fujiwara, S. C. Jeong, W. Galster, S. M. Lee, Y. Nagashima, T. Mikumo, H. Ikezoe, K. Ideno, Y. Sugiyama, and Y. Tomita, Z. Phys. A **335**, 203 (1990).